ISSN No: 2348-4845
International Journal & Magazine of Engineering, Technology, Management and Research
A Peer Reviewed Open Access International Journal

# A Set of Multilevel inverters to generate 10-MW from Wind Turbines

**Mr.V.Rajesh**
M.Tech (Power Electronics)
Dhruva Institute and Technology
Nalgonda, Telangana 508252

**Mr.V.Balu**
Assistant Professor
Dhruva Institute and Technology
Nalgonda, Telangana 508252

**Abstract:**

***Medium-voltage power conversion is generallyfavored for future large wind turbines, e.g., 10 MW, in terms ofhigher power density, reduced current level, associated losses, andcost of power cables, switchgears, etc. This paper has summarized afundamental rule to construct multilevel modular high powerconverters for large wind turbine power conversion. Based on that,three potential multilevel modular high power converter topologiesare derived and compared. The topology with a 10-kV generator, amodular power converter, and a multi-winding step-up transformerhave been specifically investigated. The large dc-link capacitor(not reliable, high cost, large volume) required in the converteris identified as the key limitation of the system used for wind powerconversion. The paper proposes to compensate the ripple powerby the grid-side inverter of the multilevel modular converter, thusreducing the dc-link capacitor requirement. The paper has validatedthe effectiveness of proportional–integral–resonant controllerfor this purpose. Further, the thermal impact of the proposed ripplepower compensation scheme on the converter device junctiontemperature and the transformer secondary windings has beenanalytically derived. The paper has also analytically revealed thatthe proposed ripple power compensation scheme will not affectthe grid-side power quality, although there are low-frequencyharmonics in the transformer secondary windings. Simulationresults with a 10-MW, 10-kV system have validated the proposedconverter topology and control strategy with reduced dc-link voltageripple***.

## I. INTRODUCTION

T ODAY, the most popular large variable-speed wind turbinesare rated around 1.5–3 MW. Nevertheless, 7-MWwind turbines have recently appeared and even larger windturbines, e.g., 10MW, are under development in order to reducethe unit cost of wind power generation [1], [2]. Wind turbinesequipped with direct-drive permanent magnet generators(PMGs) and full power converters are generally favored due tosimplified drive train structure and thus higher reliability, especiallyfor offshore applications, compared with the doubly fedinduction generator-based system. Most of the present windgenerator and power converter systems are based on the690Vand two-level voltage–source or current–source convertersare normally used [3], [4]. The continuous increase in windturbine power ratings will generate larger current, e.g., from1673 A for 2-MW system to 8810 A for 10-MW system. Powerconverters are therefore connected in parallel to handle theincreasing current [5], [6]. Meanwhile, large current transferresults in a parallel connection of multiple power cables goingdown through the tower and causes substantial losses ( ),voltage drop, as well as high cost of cables, switchgears, andterminal connections [7]. These disadvantages can be offset byplacing the step-up transformer (e.g., 690 V/33 kV) into thenacelle. However, the bulky and heavy transformer occupies thelimited space of the nacelle and increases the mechanical stress ofthe tower. Therefore, a medium-voltage power conversion system(e.g., 10 kV) would be more desirable for large wind powerconversion by reducing the current level and associated cablecost and losses, as well as improving the system power density.The benefits of adopting medium-voltage power conversiontechnology have been proved in motor drive applications, wheremedium-voltage (3–33 kV) configuration is generally used whenthe system power rating is higher than 1 MW [8]. Table I showsthe current rating of an exemplar 5- and 10-MW systems with690-V and 10-kV voltage level for comparison. As seen, transferringfrom low voltage (690 V) to medium voltage (10 kV) cansignificantly reduce the current level. Further, considering thehigh maintenance cost and fault-tolerant requirement especiallyfor offshore wind applications, a modular converter and generatorstructure is even preferable.

Regarding medium-voltage multilevel converter topologiesfor wind power applications, papers [9]–[12] investigate thesuitability of three-level neutral-point-clamped converters.Although a higher voltage rating and reduced output harmonicsare achieved, the ac-side voltage is limited to 4.0 kV if using4.5-kV integrated gate-commutated thyristors (IGCTs) [11]. Thevoltage rating may be further increased if using 6-kV IGCT;however, the cost and availability becomes a major concern. Afive-level hybrid converter topology with increasing number ofdevices is presented in [13] to further increase the convertervoltage and power capability. However, the reliability restricts itsapplication. If one device fails, the whole converter systemoperation may be interrupted. A more applicable way to achieve6- or 10-kV medium-voltage power conversion is through thecascaded modular converter structure [2], [8]. The voltage levelcan be easily scaled up by cascading more converter cells. Papers[14]–[18] have proposed various converter topologies based onthis concept. However, the fundamental connections betweenthese topologies are not analyzed. The cascaded convertertopology has intrinsic fault-tolerant operation capability. If onecell fails, it can be bypassed and the rest healthy cells can keepoperation [17]. One of the main disadvantages of the cascaded

TABLE I
WIND TURBINE CURRENT RATING FOR DIFFERENT VOLTAGE LEVELS

| Wind turbine power (MW) | Voltage (kV) | Current (A) |
|---|---|---|
| 5.0 | 0.69 | 4400 |
| | 10 | 303 |
| 10 | 0.69 | 8810 |
| | 10 | 607 |

Converter topology is the large dc-link capacitor required to filterthe dc-link voltage ripple from the H-bridge side in each cell [14],[19]. The dc-link capacitor is unreliable and is not favored inwind power applications where maintenance cost is very high.There are no effective solutions to significantly reduce the dclinkcapacitor. In motor drive applications, diode rectifiers arenormally used, which cannot be actively controlled to compensatethe ripple power thus reducing the dc-link capacitor.

In this paper, a fundamental rule to construct multilevelmodular high power converters for large wind turbine powerconversion is proposed. Based on this, three potential multilevelmodular wind power converter topologies have been derivedusing a generalized approach for an exemplar 10-kV, 10-MWwind turbine. A special focus has been given to the topologycomprising a 10-kV generator, a multilevel modular converter,and a multi-winding grid-side transformer. A solution to reducethe dc-link capacitor is proposed by compensating the ripplepower from the three-phase grid-side inverter. A resonant controlleris presented to achieve this purpose. The current harmonicsinduced in the inverter and transformer secondary windingsby the proposed control scheme and their impact are alsoinvestigated analytically. The converter topology and dc-linkcapacitor reduction strategy has been simulated and validatedwith a 10-kV, 10-MW wind power conversion system, where thedc-link voltage ripple is effectively attenuated without affectingthe grid power quality.

## II. 10-kV, 10-MW WIND POWER MODULARCONVERTER TOPOLOGIES

ISSN No: 2348-4845
International Journal & Magazine of Engineering, Technology, Management and Research
A Peer Reviewed Open Access International Journal

As mentioned, one of the most applicable and economic wayto achieve a 10-kV power conversion system is through seriesconnection of modular converter cells. In particular, 3.3-Kvinsulated-gate bipolar transistor (IGBT) device is considered inthis application due to their better availability and lower cost,compared with 4.5- and 6-kV devices. Fig. 1 shows a generalizedphase leg of a cascaded modular converter structure. The outputsof several converter cells (ac/dc/ac) are connected in series toachieve high-voltage output. With 3.3-kV IGBTs, 10-kV linevoltageoutput can be achieved with five stages, where eachmodule dc-link voltage is regulated at around 1800 V, thus3.3-kV devices can be used. It should be noted that the convertermodules in Fig. 1 cannot be directly connected in series at bothends without isolation. A galvanic isolation is needed in eachconverter module in order to cascade the outputs at either end.There are three possible locations to place the isolation, viz., atthe generator side (I), in the dc link (II), or at the grid side (III), asshown in Fig. 1. The isolation can be achieved through eithergenerator isolated windings, high-frequency transformer in thedc-link or multi-winding grid-side transformer. Based on this,

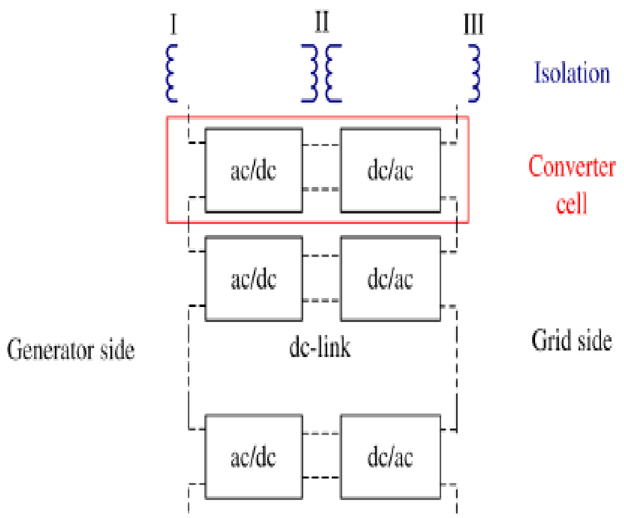


Fig.1. Generalized cascaded multilevel converter topology (one phase leg).

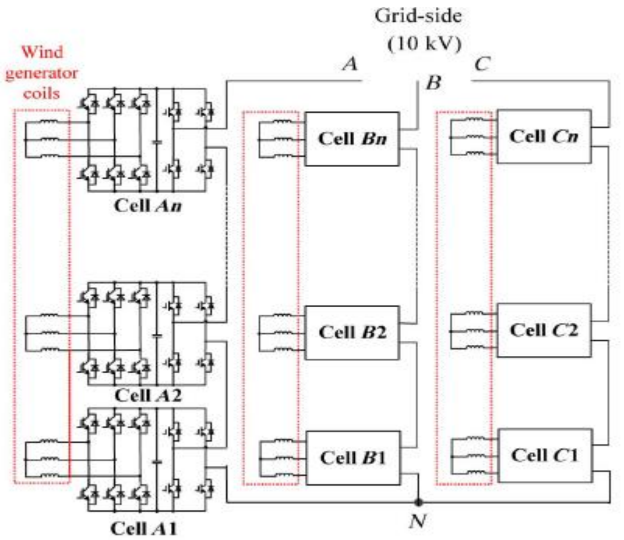


Fig.2. High-power, medium-voltage (10 kV) modular wind converter withgenerator-side isolation (converter type I).

three potential high-power, medium-voltage modular wind convertertopologies are given in Figs. 2–4, respectively.

Fig. 2 shows a high-power, medium-voltage (10 kV) windconverter topology (type I) by using the generator-side isolation.The isolated coils in the generator stator windings are connectedout separately to provide independent power sources for eachconverter cell. The input power stage of each cell is a three-phaseactive rectifier and the output stage is an H-bridge inverter. Theoutputs of each H-bridge are connected in series to achieve highvoltage (e.g., 10 kV) at the grid side. This topology requires thegenerator to provide multiple three-phase coils. The direct-drivePMGs generally have many pole pairs, where the correspondingthree-phase coils of each pole pair (or several pole pairs connectedin series or in parallel, depending on the required voltagerating) can be connected out separately to meet this requirement.Regarding the control, the input three-phase rectifier is responsiblefor regulating the dc-link voltage of each converter cell andthe grid-side cascaded H-bridge converter regulates the activepower [e.g., for maximum power point tracking (MPPT)] andreactive power fed into the grid [14], [16]. With

ISSN No: 2348-4845
International Journal & Magazine of Engineering, Technology, Management and Research
A Peer Reviewed Open Access International Journal

this topology, thegenerator and converter are suggested to put on top of the windtower. A step-up transformer from 10 kV to the voltage level

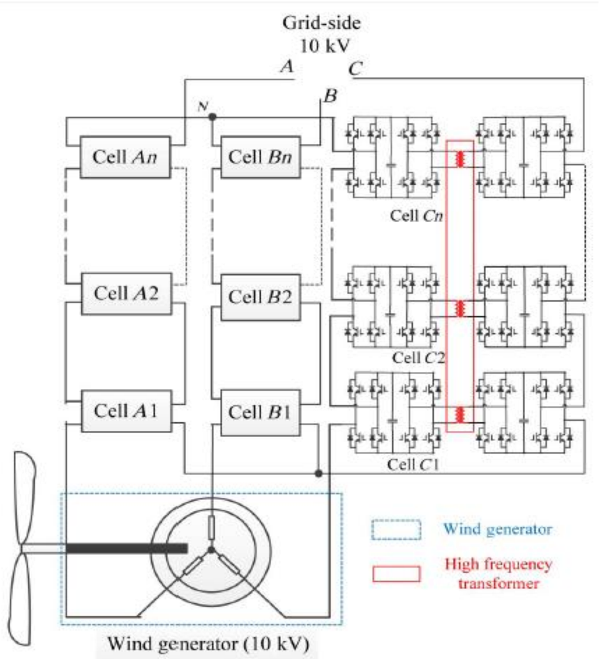


Fig.3. High-power, medium-voltage (10 kV) modular wind converter with highfrequencytransformer isolation (converter type II).

(e.g., 33 kV) of the collection point of the wind farm may berequired and can be placed at the bottom of the tower. Alternatively,a transformer-less structure may be enabled if the numberof cascaded stages can be increased to directly meet the collectionpoint voltage. It should be noted that the increased number ofgenerator terminal connections may add extra labor and maintenancecost. A dedicated generator design and wire connectionarrangement may be required.

Fig. 3 shows a second wind converter topology (type II) with ahigh-frequency transformer as the isolation, which is insertedinto the dc link together with a back-to-back H-bridge converter.This high-frequency isolation unit is also called dual activebridge (DAB) converter, where the two H-bridge converters atboth sides of the high-frequency transformer operate at a higherfrequency (e.g., several kHz), thus the size and weight of thetransformer can be significantly reduced compared with the linefrequency(50 or 60 Hz) transformer [20], [21]. The input andoutput stages of each converter cell are H-bridge converters (withthe DAB converter in between). A standard three-phase 10-kVgenerator is used and the H-bridge converters are cascaded atboth the generator side and grid side to achieve 10-kV voltagecapability thus regulating the generator and grid power. The turnsratio of the high-frequency isolation transformer can be adjusted(1:1 or 1: *n*) to achieve the desired voltage level. The powerconverter can be put flexibly either on top of the tower or at thebottom since 10-kV voltage is achieved at both ends of theconverter. The main concern with this topology is the extra lossescaused by the inserted DAB converter and high-frequencytransformer, which may be mitigated by using advanced magneticmaterial, soft-switching topologies and new wide-bandgappower devices, e.g., silicon-carbide (Sic) based device.

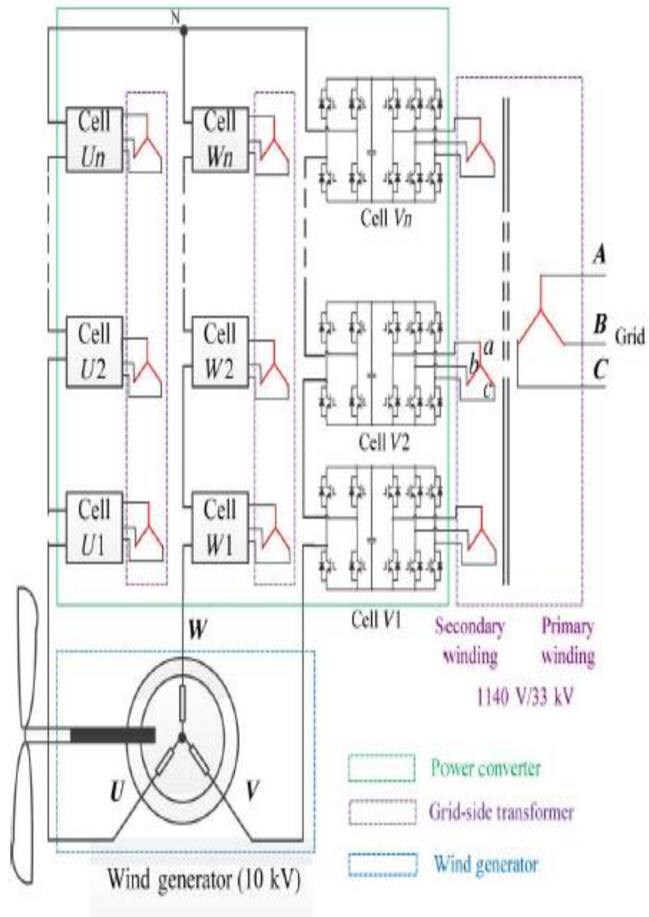


(a)

ISSN No: 2348-4845
International Journal & Magazine of Engineering, Technology, Management and Research
A Peer Reviewed Open Access International Journal

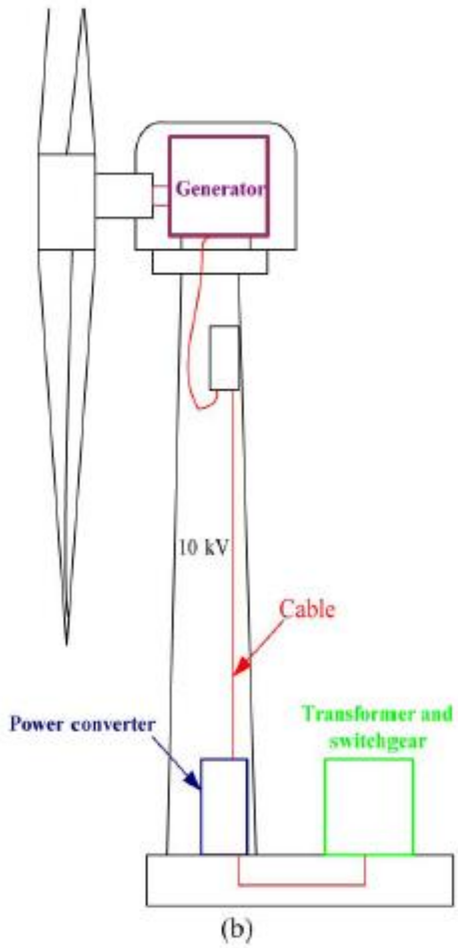


Fig.4. High-power, medium-voltage (10 kV) modular wind converter with gridsidetransformer isolation (converter type III): (a) generator and converterstructure and (b) wind turbine electrical configuration.

Fig. 4(a) shows another high-power, medium-voltage windconverter topology (type III) with a grid-side isolation transformer,which will be further investigated in this paper. As can beseen, this topology adopts a standard 10-kV wind generator and agrid-side step-up transformer with multiple secondary windings(1140 V/33 kV), which provides isolation of each converter celland also boosts the converter voltage to the grid voltage of 33 kV.The power converter and the transformer can be put at the bottomof the tower as shown in Fig. 4(b), which reduces the mechanicalstress of the tower and saves the space in the nacelle. The inputstage of each converter cell is an H-bridge rectifier which is thenconnected in series to achieve 10-kV voltage capability to controlthe generator. The output stage of each converter cell is a threephaseinverter and is connected to the transformer secondarywindings, responsible for regulating the dc-link voltage. Similarto the previous two topologies, this modular structure benefitsfrom fault-tolerant capability, when one cell fails, it can bebypassed by a switch connected in parallel to the H-bridgeconverter output and the remaining health cells can still maintainoperation subject to the reduce of power output. In view ofthe successful applications of the cascaded H-bridge converterin high power motor drive area, this topology may become astrong candidate for future large wind turbine power conversionsystems [22].

It should be noted that the low-frequency single-phase fluctuatingpower at the input stage of each cell (H-bridge) in Fig. 4(a)will cause dc-link voltage ripple, which gets larger with lowergenerator stator frequency and higher power level. For variablespeed,direct-drive PMGs, the stator frequency is generally low(e.g., below 15 Hz). Therefore, large dc-link capacitance isrequired to smooth out the voltage ripple appeared on the dclink, which are bulky and significantly increase the system cost aswell as cause reliability issues due to the lifetime of electrolyticcapacitors. This issue also happens to the other two topologies inFigs. 2 and 3. In Section IV, a solution to reduce the dc-linkcapacitance will be introduced in a later session.

## III. 10-MW WIND TURBINESPECIFICATIONS AND CONVERTER CONTROL STRATEGY

### A. 10-MW Wind Turbine Specifications

A 10-kV, 10-MW wind turbine and its PMG parameters aredesigned. The rated speed of the wind turbine is 10 rpm at windspeed of 12 m/s [23]. The PMG has 90 pole pairs, correspondingto 15-Hz stator frequency at rated speed. Fig. 5 shows thecaptured wind power variation with the generator speed. Thewind turbine control should aim to capture

ISSN No: 2348-4845
International Journal & Magazine of Engineering, Technology, Management and Research
A Peer Reviewed Open Access International Journal

maximum windpower by regulating the generator speed/power following MPPTunder normal conditions.

### B. Generator and Cascaded H-Bridge Converter ControlStrategy

The wind generator (PMG) shown in Fig. 4(a) can be modeledin a synchronous rotating ( , ) frame [3], [24]. With rotor fluxorientedcontrol, the PMG torque can be controlled by the –axiscurrent, while the -axis current is controlled to maximize thegenerator efficiency. In order to achieve MPPT, the generatortorque reference is set as the product of the optimal coefficientand the square of generator speed [25]. The standard phaseshiftedpulse width modulation (PWM) is adopted to modulatethe cascaded H-bridge converters, thus generating the requiredvoltage according to the voltage reference.

### C. Grid-Side Inverter Model and Control Strategy

At the grid side, the three-phase inverter in each converter cellas shown in Fig. 4(a) is responsible for regulating the convertercell dc-link voltage, transferring the active power generated fromwind generator to the grid. Since the inverter current is actively

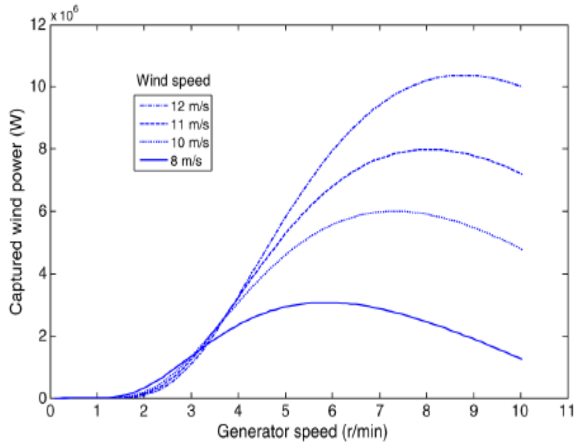


Fig.5. Variation of captured wind power with generator speed under differentwind speeds.

controlled to be sinusoidal, the topology in Fig. 4(a) does notNeed multiple phase-shifted transformer secondary windings(Zigzag winding) for harmonics reduction as the case in motordrive applications with diode rectifier, leading to a simplifiedtransformer design. The transformer leakage inductance can befurther used as the filter inductance. The model of the grid-sidethree-phase inverter in each cell on frame is given asfollows [3], [14]:

$$\begin{cases} L_e \frac{di_d}{dt} = -R_e i_d + \omega_e L_e i_q - S_d + u_d \\ L_e \frac{di_q}{dt} = -R_e i_q - \omega_e L_e i_d - S_q + u_q \end{cases} \quad (1)$$

Where*Le* and*Re* are the transformer leakage inductance andresistance;*ud*,*uq*,*id*,*iq* are the voltages and currents on thetransformer secondary side in the*d*,*q* frame, respectively; are the output voltages of the three-phase inverter in the switchingaverage model; andωe is the grid line frequency.

If the -axis of the rotating frame is aligned to the transformersecondary voltage vector, then*uq=0*and *u*d=E where E isthe amplitude of the transformer secondary voltage. The converteractive powerP and Qreactive power can be formulated by

$$\begin{cases} P = \frac{3}{2}(u_d i_d + u_q i_q) = \frac{3}{2} E i_d \\ Q = \frac{3}{2}(u_d i_q - u_q i_d) = \frac{3}{2} E i_q . \end{cases} \quad (2)$$

As seen, the active and reactive power flowing into the grid canbe controlled by -axis and -axis currents independently. Thegrid-side three-phase inverter control diagram is shown in Fig. 6.The outer loop is the dc-link voltage control loop which is kept tobe 1800 V and inner loops are -axis and -axis current controlloops. The -axis current can be used to provide reactive power tothe grid when required subject to the current capability of theconverter.

## IV. CONVERTER DC-LINK VOLTAGE RIPPLE REDUCTION

### A. Resonant Controller Added in the Control Loop

One particular issue with the converter topology shown inFig. 4(a) is the large dc-link capacitor required in each cell tosmooth the single-phase pulsating power from the H-bridge(generator) side, which can be expressed as

ISSN No: 2348-4845
International Journal & Magazine of Engineering, Technology, Management and Research
A Peer Reviewed Open Access International Journal

$$\begin{aligned} p_{g\_single}(t) &= v_{o,U}(t)\cdot i_{o,U}(t) = V_{om}\cos(\omega_o t)\cdot I_{om}\cos(\omega_o t-\varphi) \\ &= \frac{V_{om}I_{om}}{2}\cos\varphi + \frac{V_{om}I_{om}}{2}\cos(2\omega_o t-\varphi) \\ &= P_{avg}\cdot\cos\varphi + P_{avg}\cdot\cos(2\omega_o t-\varphi) \qquad (3) \end{aligned}$$

Where $V_{om}$ and $I_{om}$ are the amplitudes of the generator voltage(*u*o, u) and current (*Io, U*) seen at each cell, respectively. $P_{avg}$Is theaverage power flowing into the converter cell ωo is the generatorstator frequency andφ is the generator power factor angle.As seen, the second term in (3) represents the pulsating powerwith the frequency of 2ωo, which causes dc-link voltage ripple.The amplitude of dc-link voltage ripple $\Delta$V can be expressed as

$$\Delta V = \frac{P_{avg}}{\omega_o\cdot C\cdot V_{dc}} \qquad (4)$$

WhereC is the dc-link capacitor andVdc is the dc-link voltage.As seen, the dc-link voltage ripple becomes larger with lowergenerator frequency and higher power rating. To keep the dc-linkvoltage ripple within $\Delta$V, the required dc-link capacitanceC canbe calculated by

$$C \geq \frac{P_{avg}}{\omega_o\cdot \Delta V\cdot V_{dc}}. \qquad (5)$$

For a 10-MW wind power converter with 15 cells (5 stages),1800-V dc-link voltage, and 15-Hz generator stator frequency,the required capacitor in each cell will be 44 mF in order to keepthe voltage ripple to be within 5% (90 V) at the rated operatingpoint.

To achieve such large capacitance at this voltage level, manyelectrolytic capacitors need to be connected in both series and inparallel, which are not only expensive and bulky, but also causereliability issues of the system, since the electrolytic capacitorhas almost the highest failure rates in a typical wind powerconverter system [26]. For offshore applications, high reliabilityis a key to reduce the maintenance cost.

Therefore, an effectivemethod to reduce the required dc-link capacitor is critical. Due tothe use of controlled three-phase inverter in each cell, the powertransferred to the transformer secondary winding can be welladjusted to compensate the power ripple from the H-bridgerectifier. If the power of the three-phase inverter in (2) isregulated the same as the power from the H-bridge rectifier asin (3) (including the pulsating power), in theory, no dc-linkcapacitor is required to handle the low-frequency (2ωo) powerripple.

By equating (2) with (3), the inverter -axis current becomes(6) under vector control

$$\begin{cases} i_{d,U} = \frac{V_{om}I_{om}}{3E}\left[\cos\varphi + \cos(2\omega_o t-\varphi)\right] \\ i_{q,U} = 0 \end{cases} \qquad (6)$$

Where*id*,U and*iq*,*U*are -axis and -axis currents assuming thatthe three-phase inverter is connected to phase*U* of the generator.As can be seen, the -axis current has an ac component with the

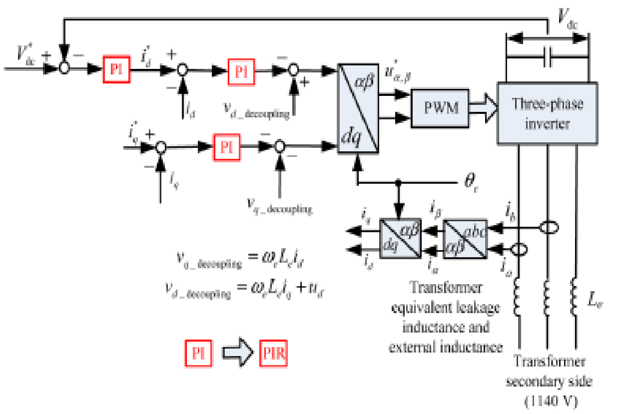


Fig.6. Vector control diagram of the grid-side inverter in each cell (The PIcontroller is replaced with a PIR controller when the dc-link voltage ripplereduction function is enabled.).

Frequency2ωoof, which is different from the conventionalcontrol where only dc component exists. If the -axis current of the three-phase inverter can be controlled the same as in (6), then there will be no dc-link lowfrequencyvoltage ripple in steady state.

ISSN No: 2348-4845
International Journal & Magazine of Engineering, Technology, Management and Research
A Peer Reviewed Open Access International Journal

However, the conventionalproportional–integral (PI) controllers used in standarddc-link voltage and current loops in Fig. 6 can only guaranteezero steady-state error for dc component, not at twice of thegenerator stator frequency (2ωo ). Therefore, a proportional–integral–resonant (PIR) controller is introduced here to replacethe PI controller thus regulating the pulsating power2ωo atfrequency. The resonant frequency of R-controller is set at 2ωo. The transfer function of the PIR controller is given as follows[27], [28]:

$$G_{\mathrm{PIR}}(s) = K_p + \frac{K_i}{s} + \frac{2K_r s}{s^2 + (2\omega_o)^2} \qquad (7)$$

Where KP,K*i*, and are the proportional, integral, and resonantcoefficients, respectively.

The selection ofKP andK*i* will follow the standard currentloopdesign process to achieve a desirable control bandwidth.Based on the grid-side inverter model in (1), the -axis currentloopplant model can therefore be expressed as

$$\frac{I_d(s)}{S_d(s)} = \frac{1}{sL_e + R_e} \qquad (8)$$

Where $\omega_e L_e i_q$ and $u_d$ are treated as cross-coupling terms. If $K_p$ ischosenas $\omega_c L_e$ and $K_i$ is chosen as $\omega_c R_e$, where $\omega_c$ is thedesigned current-loop bandwidth, the closed-loop transfer functionwill become

$$\frac{I_d^*(s)}{I_d(s)} = \frac{\omega_c}{s + \omega_c}. \qquad (9)$$

It can be seen that the closed-loop transfer function is a firstordersystem with a bandwidth of $\omega_c$ . The -axis current-loopdiagram is shown in Fig. 7.

The selection of*Kr* is to make sure that there is sufficient gainat the resonant frequency to reduce the low-frequency currentripple. In theory, since the resonant controller has infinite gain at

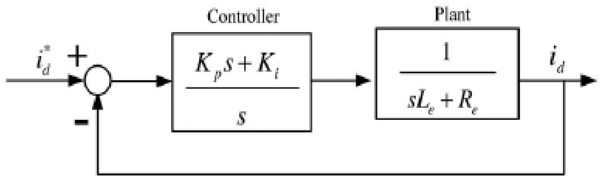


Fig.7. Current-loop diagram with a PI controller

the resonant frequency,*Kr* can be any positive value (e.g.,*Kr*> 1). However, in digital implementation, due to discretizationeffect, the gain at the resonant frequency may be limited.Therefore, a larger*Kr* value is preferred. It should also be notedthat if the *Kr*value is too large, the stability of the system may beaffected especially when the resonant frequency is close to thecurrent-loop cross-over frequency.

Fig. 8 shows the open-loop and closed-loop frequencydomain response of using PI and PIR controllers for comparison.The current-loop bandwidth $\omega_c = 300\ \mathrm{Hz}, R_e = 0.01\ \Omega, L_e = 1\ \mathrm{mH}$ therefore, KP= 0.3,Ki = 3 the resonant frequency $2\omega_o$ = 100Hz and *Kr=100.*

As seen, the resonant (R) controller creates an infinite gain atthe resonant frequency (100 Hz). In the closed loop, this convertsto unity gain and zero phase delay at the resonant frequency,which means the real current can follow the reference accurately.Therefore, the ripple power can be effectively compensated andthe dc-link voltage ripple is reduced. The design of the PIRcontroller for the voltage loop can follow the same process.

ISSN No: 2348-4845
International Journal & Magazine of Engineering, Technology, Management and Research
A Peer Reviewed Open Access International Journal

In addition, considering the accuracy of the generator Frequency/speed measurement, it is desirable to have a certaintolerance when setting the resonant frequency. Therefore, abandpass controller/filter can be used, instead of the pure resonantcontroller. This will improve the robustness of the controllerespecially when there is small error in the frequency measurement.The bandpass controller will also avoid the stability issuescaused by the infinite gain of the resonant controller at theresonant frequency. The transfer function of the band pass filteris given as follows:

$$G_{\mathrm{R\_BP}} = \frac{2K_r\omega_b s}{s^2 + 2\omega_b s + {\omega_o}^2} \quad (10)$$

Where is$\omega o$ the center frequency of the bandpass filter and$\omega b$ isthe bandwidth of the bandpass filter. The bandpass filter has ahigh, but limited gain at the resonant frequency$\omega o$, which can befurther tuned by the resonant gain*Kr*.

Note that the resonant frequency varies with the generatorfrequency/speed. Therefore, the generator frequency informationneeds to be fed to the PIR controller to set the resonantfrequency.

It should also be noted that on using this dc-link voltage ripplereduction scheme, the power transferred to the transformersecondary winding in each cell will contain a power ripple,instead of a constant power. As a result, the three-phase invertercurrent (transformer secondary-winding current) is not sinusoidaland contains harmonics. However, these current harmonicsare canceled with each other among the transformer secondarywindings and do not appear at the transformer primary-side/grid-side (33 kV) and therefore would not affect the grid power

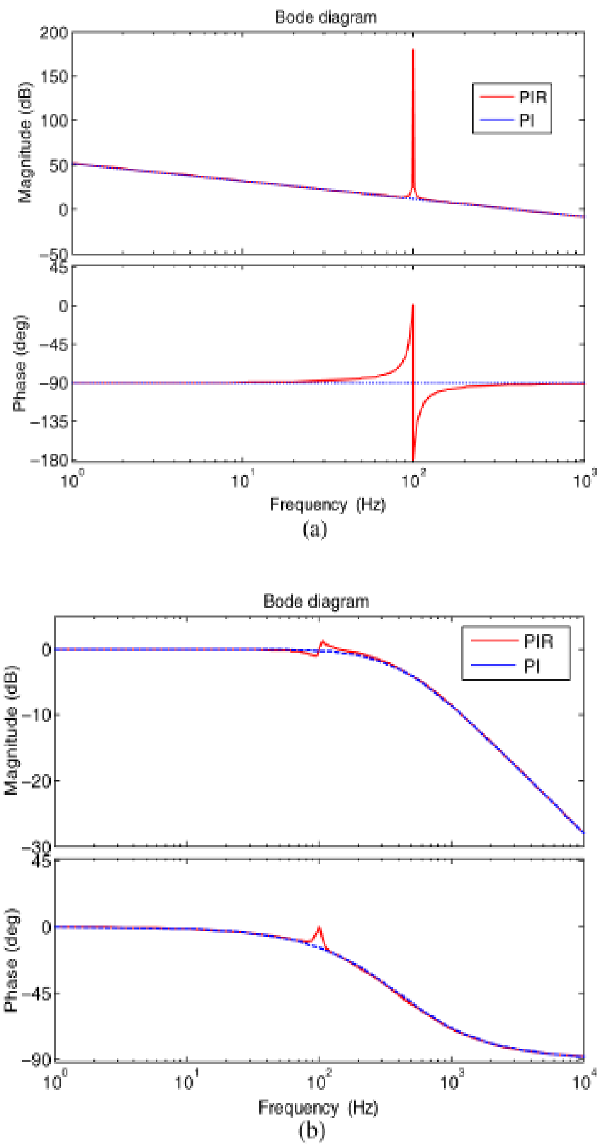


Fig. 8. Current-loop frequency response with PI and PIR controllers: (a) openloopfrequency response and (b) closed-loop frequency response.

Quality. Section IV-B will analyze the current harmonics in boththe transformer secondary and primary windings.

B. Current Harmonics Analysis

In the following analysis, the generator phases are denoted by*A*, *U*, *V*, *W*, and the transformer primary phases are denoted by A,B, C and the transformer secondary phases are denoted by a, b ,c ,respectively, as indicated in Fig. 4(a).

Connecting to the cells of generator phase*U* is given. Similarly,the corresponding -axis current of the three-phase inverters ofthe cells connected to generator phases*V* and*W* can be derivedas in (11) and (12) by considering the phase shift of 120

$$i_{d,V} = \frac{V_{om} I_{om}}{3E}\left[\cos\varphi + \cos\left(2\omega_o t - \varphi - \frac{4\pi}{3}\right)\right] \quad (11)$$

$$i_{d,W} = \frac{V_{om} I_{om}}{3E}\left[\cos\varphi + \cos\left(2\omega_o t - \varphi + \frac{4\pi}{3}\right)\right]. \quad (12)$$

To analyze the current harmonics in the three-phase inverter,the , currents given in (6), (11), and (12) are transformed backto , , coordinate by using inverse-Park transformation. For thecells connecting to phase*U* of the generator, the inverter phase*a*current (transformer secondary current) can be expressed as

$$\begin{aligned} i_{a,Ui} &= \frac{V_{om} I_{om}}{3E}[\cos\varphi + \cos(2\omega_o t - \varphi)]\cos(\omega_e t + \theta_{0,Ui}) \\ &= \frac{V_{om} I_{om}}{3E}\left\{\begin{array}{l} \cos(\omega_e t + \theta_{0,Ui})\cos\varphi \\ +\frac{1}{2}\cos[(\omega_e + 2\omega_o)t + (\theta_{0,Ui} - \varphi)] \\ +\frac{1}{2}\cos[(\omega_e - 2\omega_o)t + (\theta_{0,Ui} + \varphi)] \end{array}\right\} \end{aligned} \quad (13)$$

where*ia,Ui* represents the phase current of the inverter and thesuffix*U* denotes the inverter cell which is connected to phase*U*of the generator. Suffix*i*denotes the *i*th module of the modulestring.θ0, *Ui* is the phase angle of the transformer secondaryvoltage ωe and is the grid frequency. As seen from (13), theinverter phase current (transformer secondary current) containsnot only the fundamental component with the grid frequency ofωe, but also the frequency componentsωe +2ωo of andωe -2ωo. These current harmonics are due to the compensationofthe power ripple from the H-bridge side.

Similarly, the inverter phase current of the cells connected togenerator phases V and W can be expressed as in (14) and (15),respectively,

$$i_{a,Vi} = \frac{V_{om} I_{om}}{3E}\left\{\begin{array}{l} \cos(\omega_e t + \theta_{0,Vi})\cos\varphi \\ +\frac{1}{2}\cos\left[(\omega_e + 2\omega_o)t + \left(\theta_{0,Vi} - \varphi - \frac{4\pi}{3}\right)\right] \\ +\frac{1}{2}\cos\left[(\omega_e - 2\omega_o)t + \left(\theta_{0,Vi} + \varphi + \frac{4\pi}{3}\right)\right] \end{array}\right\} \quad (14)$$

$$i_{a,Wi} = \frac{V_{om} I_{om}}{3E}\left\{\begin{array}{l} \cos(\omega_e t + \theta_{0,Wi})\cos\varphi \\ +\frac{1}{2}\cos\left[(\omega_e + 2\omega_o)t + \left(\theta_{0,Wi} - \varphi + \frac{4\pi}{3}\right)\right] \\ +\frac{1}{2}\cos\left[(\omega_e - 2\omega_o)t + \left(\theta_{0,Wi} + \varphi - \frac{4\pi}{3}\right)\right] \end{array}\right\} \quad (15)$$

Whereθ0,θ0Wi are the voltage phase angles of the transformersecondary windings of the cells connected to the generatorphases V, W, respectively. In the converter and transformerconfiguration shown in Fig. 4(a), all the transformer secondaryvoltages have the same phase angle with respect to the primary side .Therefore, $\theta_{0,Ui} = \theta_{0,Vi} = \theta_{0,Wi} = \theta_{0,i}$

If the inverter phase*a* currents of the cells connected togenerator phases *U*, *V*,*W*, as shown in (13)–(15), are addedtogether, the total phase current becomes

$$i_{a,Ui} + i_{a,Vi} + i_{a,Wi} = \frac{V_{om} I_{om}}{E}\cos(\omega_e t + \theta_{0,i})\cos\varphi. \quad (16)$$

As seen, the harmonic currents with the frequency ofωe +2ωoandωe -2ωo in each cell are canceled among the transformersecondary side. Therefore, they do not exist in the transformerprimary. The transformer primary side (grid side) only containsthe fundamental sinusoidal component with the frequencyofωe.The same current harmonics analysis can be done for phasesand*b*. Therefore, the proposed dc-link capacitance reductionmethod does not affect the grid power quality, although thetransformer

ISSN No: 2348-4845
International Journal & Magazine of Engineering, Technology, Management and Research
A Peer Reviewed Open Access International Journal

secondary-side (inverter) will have current harmonicsofωe +2ωoandωe -2ωo.

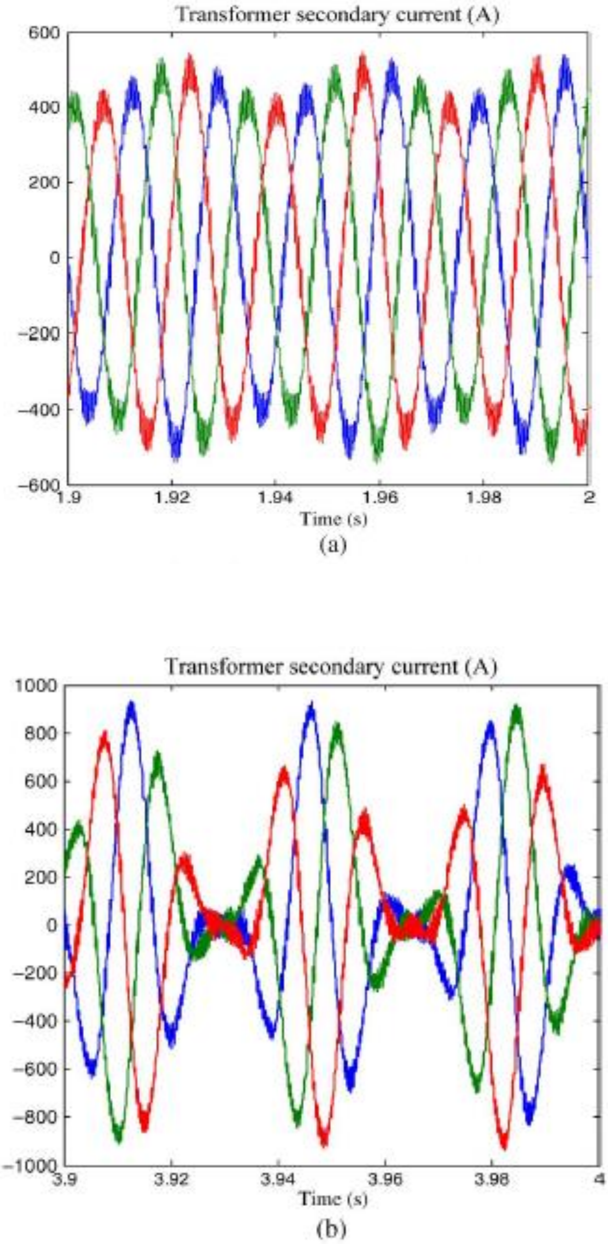


Fig.9. Inverter (transformer secondary) current with and without resonantcontroller applied: (a) without resonant controller and (b) with resonantcontroller.

## C. Inverter and Transformer Power Losses Analysis

While the low-frequency power ripple from H-bridge side canbe effectively compensated from the transformer-side inverter,the harmonic current may cause extra thermal stress to theinverter power devices and the transformer secondary windings.Fig. 9 shows the simulated inverter current waveform with andwithout the dc-link voltage ripple reduction method applied for a10-MW system at a rated wind speed. As seen, with the dc-linkripple reduction method applied, the peak current (due to theharmonics) of each phase may double the value of the currentwithout compensation. The exact expression of the currentwaveform is given in (13)–(15) for phase. Therefore, thepower device current rating should be chosen to meet the peakcurrent requirement.

In order to evaluate the thermal performance and the impact ofthe control algorithm on the inverter, the inverter losses anddevice junction temperature are calculated and simulated. For a10-MW, 10-kV generator, the rated root mean square (RMS)current is 577 A. With a 1140-V/33-kV grid-side transformer and

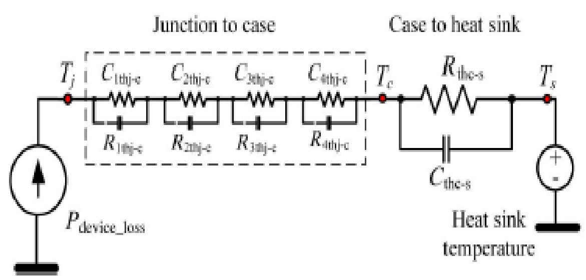


Fig.10. Thermal network to evaluate the device junction temperature.

15 converter cells, the transformer secondary winding RMScurrent is 337 A. Note that if the ripple power compensationscheme is activated, the peak of transformer secondary currentmay increase to 950 A. With these current values, IGBT modulesfrom Infineon FZ1000R33HL3 (3300 V, 1000 A) are used forboth H-bridge rectifier and the inverter to evaluate the systemthermal performance [29], [30]. The switching frequency isselected at 2 kHz.

ISSN No: 2348-4845
International Journal & Magazine of Engineering, Technology, Management and Research
A Peer Reviewed Open Access International Journal

In the simulation, the heat sink temperature is assumed to befixed at 80°C due to its large thermal time constant. The thermalnetwork is shown in Fig. 10. The thermal network comprises thejunction to case and case to heat sink thermal impedance.

Fig. 11 shows the inverter device junction temperature variation.Without ripple power compensation, the IGBT temperaturevaries between 96 and 102°C . The diode junction temperaturevaries between 94.5 and 104°C . When the ripple power compensationscheme is applied, the inverter current becomes as inFig. 9(b) and the junction temperature variation gets larger as wellas the peak temperature, although the average temperature stayssimilar with the non-compensated case. Larger junction temperaturevariation may reduce the lifetime of the power device. Thethermal design should also make sure the peak temperaturedoes not exceed the maximum allowable junction temperature.

Another impact of the ripple power compensation scheme isthe circulating harmonic current inside the transformer secondarywindings and the corresponding extra copper losses it hasintroduced. From (13), the RMS value of the transformer secondarycurrent with harmonics can be calculated as

$$\begin{aligned} I'_{a\_\mathrm{RMS}} &= \frac{V_{om} I_{om}}{3E} \cdot \sqrt{\left(\frac{1}{\sqrt{2}}\right)^2 + \left(\frac{1}{2\sqrt{2}}\right)^2 + \left(\frac{1}{2\sqrt{2}}\right)^2} \\ &= \frac{V_{om} I_{om}}{3E} \cdot \frac{\sqrt{3}}{2} \end{aligned} \qquad (17)$$

WhereI'a_RMSis the RMS value of the current including harmonics.The RMS value of the fundamental current can be calculatedas

$$I_{a\_\mathrm{RMS}} = \frac{V_{om} I_{om}}{3E} \cdot \frac{1}{\sqrt{2}}. \qquad (18)$$

Therefore, the ratio of the transformer secondary copper losswith and without the ripple power compensation scheme can becalculated as

$$\left(\frac{I'_{a\_\mathrm{RMS}}}{I_{a\_\mathrm{RMS}}}\right)^2 = \left(\frac{\sqrt{6}}{2}\right)^2 = 1.5. \qquad (19)$$

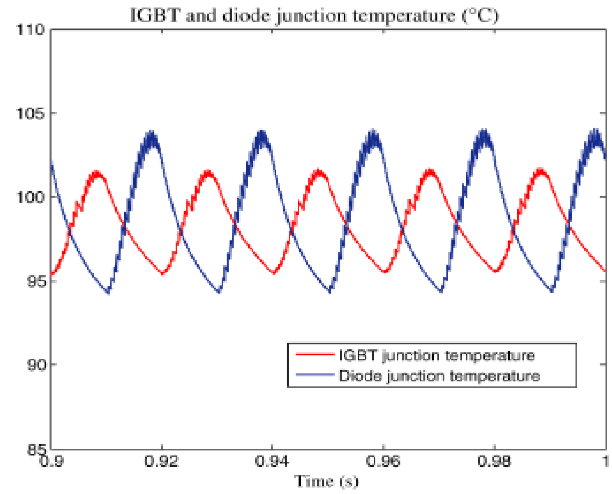

(a)

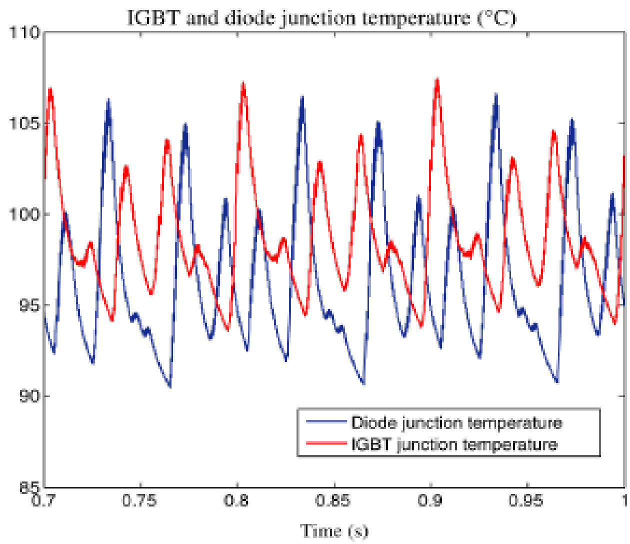

(b)

Fig.11. Inverter device (IGBT/diode) junction temperature variation: (a) withoutresonant controller and (b) with resonant controller.

ISSN No: 2348-4845
International Journal & Magazine of Engineering, Technology, Management and Research
A Peer Reviewed Open Access International Journal

As seen, the winding copper losses have increased by 50% dueto the extra harmonics, which need to be taken into considerationduring the transformer and cooling system design.

## V. SIMULATION AND RESULTS

A simulation model has been built in MATLAB/Simulink inorder to validate the converter topology in Fig. 4 and controlstrategy in Fig. 6. The power converter consists of 5 stages(15 cells), with each dc-link voltage of 1800 V. The dc-linkcapacitance is 44 mF. The wind turbine characteristics are thesame as in Fig. 5.

Fig. 12 shows the steady-state simulation results at thewind speed of 12 m/s with 10-MW wind power generation.Fig. 12(a) shows the generator-side converter output voltage,which has 11 levels and the generator current. Fig. 12(b)shows the transformer secondary winding (inverter) currents(1140-V side) in one converter cell. The grid (33 kV) phase

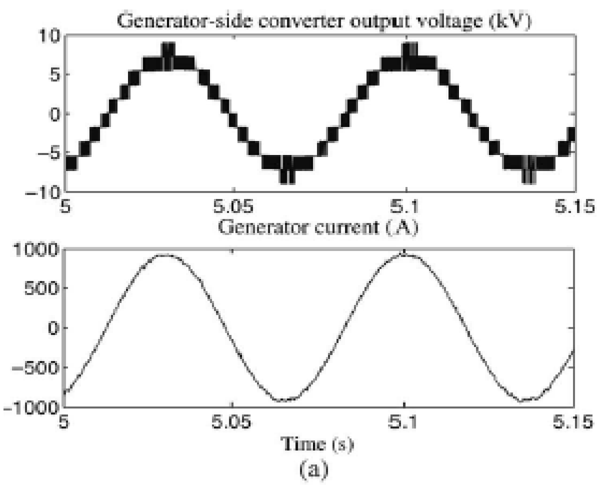


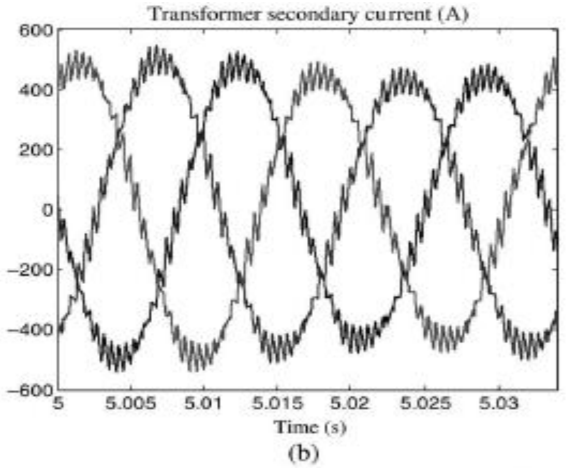


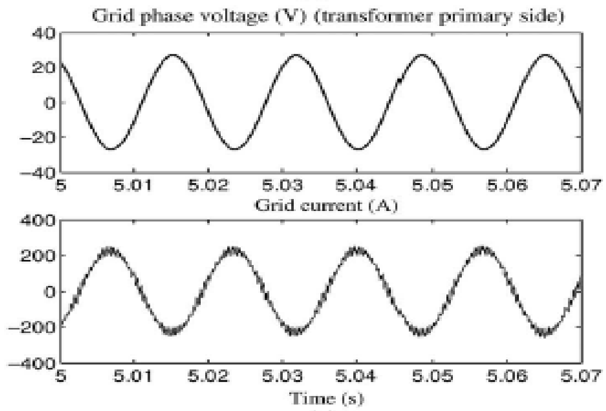


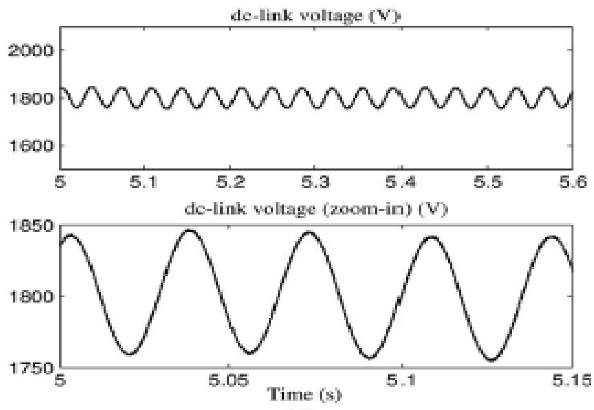


Fig. 12. Steady-state simulation results at wind speed of 12 m/s: (a) generatorsideconverter output voltage and generator current, (b) transformer secondarywinding current in a converter cell, (c) grid phase voltage and current, and(d) dc-link voltage and detailed trace.

ISSN No: 2348-4845
International Journal & Magazine of Engineering, Technology, Management and Research
A Peer Reviewed Open Access International Journal

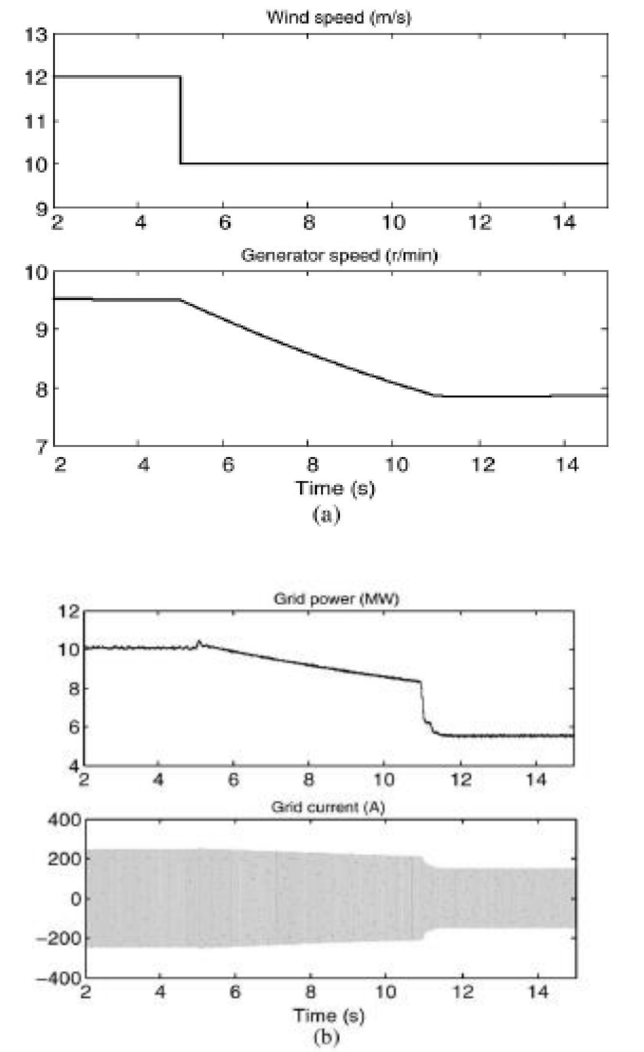


Fig.13. System response during wind speed drop from 12 to 10 m/s: (a) windspeed and generator speed and (b) power transferred to the grid and grid current.

Voltage and current are shown in Fig. 12(c). As seen, the gridcurrent is kept sinusoidal and the phase relationship betweenvoltage and current indicates wind power is fed into the grid.Fig. 12(d) shows the dc-link voltage regulated at 1800 V.With 44-mF dc-link capacitor, the voltage ripple is around90 V, which agrees with the calculated results by (4). Adetailed waveform is shown at the bottom of this figure andthe ripple frequency is 30 Hz, which is twice of the generatorfrequency of 15 Hz.

Fig. 13 shows the system response during a wind speed dropfrom 12 to 10 m/s at 5 s. The converter and generator control aimsto achieve MPPT under both wind speeds. Fig. 13(a) shows thewind speed profile and the corresponding generator speed. Asseen, the generator speed reduces from 9.5 (MPPT point for12 m/s) to 7.7 r/min to reach the MPPT point according to Fig. 5.Fig. 13(b) shows the power transferred to the grid and the gridcurrent.

Fig. 14 shows the results of dc-link voltage ripple reductionby using the PIR controller in the dc-link voltage and currentcontrol loops of each converter cell, as illustrated in thediagram in Fig. 6. To observe the effect more clearly, thedc-link capacitance has been reduced from 44 to 22 mF.Therefore, without using PIR controller, the dc-link voltageripple of each cell should be 180 V. Fig. 14(a) shows the dclinkvoltage, where the resonant controller is applied at 2 s. As

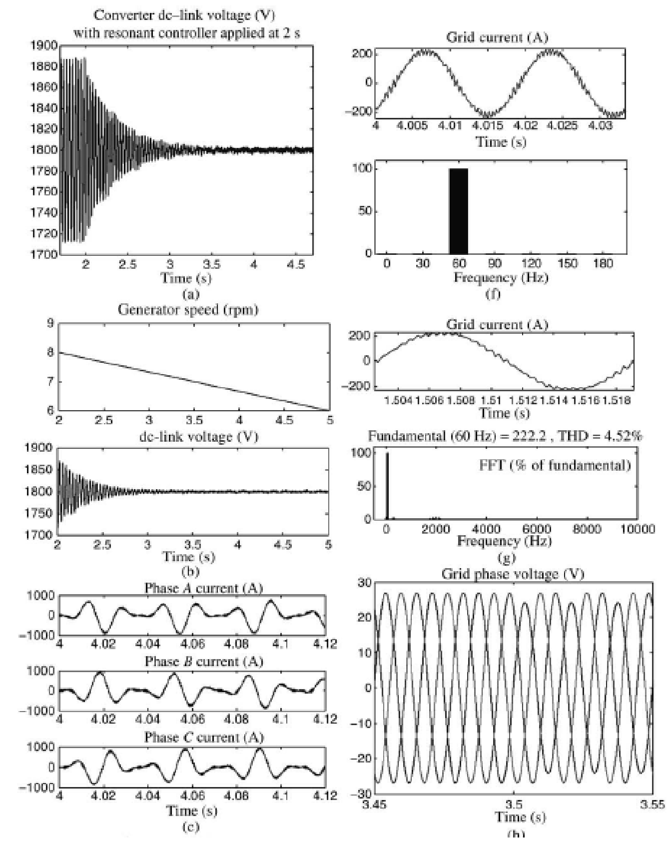

ISSN No: 2348-4845
International Journal & Magazine of Engineering, Technology, Management and Research
A Peer Reviewed Open Access International Journal

(h)

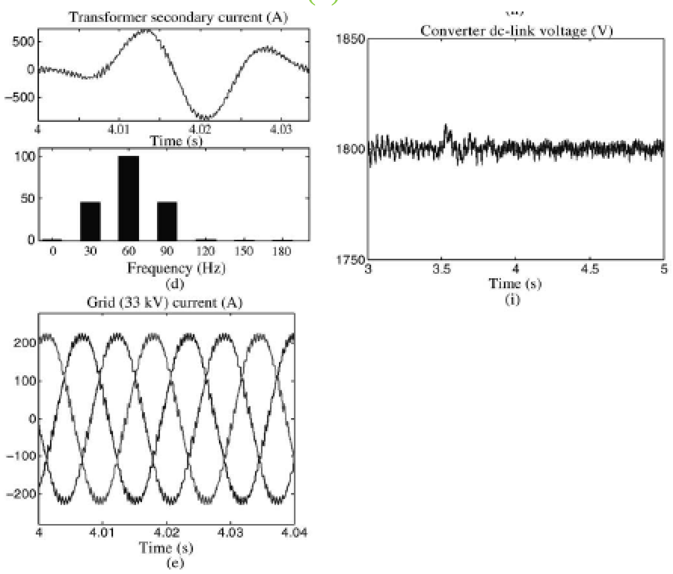


Fig. 14. Simulation results with a PIR controller engaged to reduce the dc-linkvoltage ripple: (a) converter cell dc-link voltage with resonant controller appliedat 2 s, (b) dc-link voltage during generator speed variation, (c) transformersecondary winding current, (d) FFT analysis of transformer secondary windingcurrent, (e) transformer primary (grid) current, (f) FFT analysis of transformerprimary winding current, (g) THD of the grid current, (h) grid phase voltageswith phase *A*10% drop at 3.5 s, and (i) converter dc-link voltage underunbalanced grid.

Seen, before the resonant controller is applied, the dc-linkvoltage ripple is around 180 V. After the resonant controller isapplied, the dc-link voltage ripple reduces dramatically toaround zero, which validates the proposed dc-link voltageripple reduction method. As a result, the required dc-linkcapacitor can be much smaller than that without a resonantcontroller, which can save the capacitor cost, size, as well asincrease the system reliability. Fig. 14(b) further shows theperformance of the controller during the change of generatorspeed. The resonant controller is applied at 2 s. During 2–5 sthe generator speed varies from 8 to 6 rpm and the controllereffectively adjusts the resonant frequency and attenuates thevoltage ripple regardless of the generator speed variation.Fig. 14(c) shows the corresponding transformer secondarycurrent in each cell when the resonant controller is engaged.As seen, the currents are not sinusoidal due to the compensationof the pulsation power. As analyzed in (13)–(15), thecurrent contains harmonics with frequency ofωe + 2ωoandωe-2ωo. The fast Fourier transform (FFT) analysis ofthe current is shown in Fig. 14(d),where the current contains thegrid-frequency (ωe) component of 60 Hz as well as two otherfrequency components of 90 Hz (ωe +2ωo) and 30 Hz( ) at the generator stator frequency (ωe -2ωo) of 15 Hz.Fig. 14(e) shows the transformer primary (grid)-side currentwaveform, which is sinusoidal and does not contain anylow-frequency harmonics as indicated by the FFT analysis inFig. 14(f) that only the 60-Hz grid-frequency componentappears. It is evident that the proposed dc-link voltage ripplereduction method does not affect the grid-side power quality.Fig. 14(g) shows the total harmonic distortion (THD) of the gridcurrent, which is 4.52% in this case, where the grid-interfaceinductance is 0.5 mH and the switching frequency is 2 kHz.Fig. 14(h) and (i) shows the effectiveness of the dc-link voltageripple reduction scheme under an unbalanced grid condition. At3.5 s, phase*A* voltage has a 10% voltage drop. From theconverter dc-link voltage, it can be seen that the dc-link voltageripple is effectively attenuated regardless the voltage drop in phase*A*.

## VI. CONCLUSION

In this paper, three high-power medium-voltage (10 kV)modular wind power converter topologies have been derivedbased on a generalized structure by using different formats ofisolation. A method has been proposed to attenuate the dc-linkvoltage ripple, thus reducing the capacitor requirement,by compensating the low-frequency power ripple. A PIR Controller-based control loop has been designed to achievethis purpose. The proposed dc-link voltage reduction schemewill introduce harmonics in the transformer secondary current;however, not degrading the grid power quality (sinusoidalcurrent). The current harmonics will increase the stress ofthe power devices and the transformer copper loss. Simulationresults with a 10-kV, 10-MW system have validated theconverter

ISSN No: 2348-4845
International Journal & Magazine of Engineering, Technology, Management and Research
A Peer Reviewed Open Access International Journal

topology and control scheme. The proposed dc-linkvoltage ripple reduction method may also be used in the othertwo topologies presented in the paper.

## REFERENCES

[1] M. Liserre, R. Cardenas, M. Molinas, and J. Rodriguez, "Overview of multi-MW wind turbines and wind parks," IEEE Trans. Ind. Electron., vol. 58, no. 4, pp. 1081–1095, Apr. 2011.

[2] F. Blaabjerg, M. Liserre, and K. Ma, "Power electronics converters for windturbine systems," IEEE Trans. Ind. Appl., vol. 48, no. 2, pp. 708–719, Mar. 2012.

[3] M. Chinchilla, S. Arnaltes, and J. Burgos, "Control of permanent-magnetgenerators applied to variable-speed wind-energy systems connected to the grid," IEEE Trans. Energy Convers., vol. 21, no. 1, pp. 130–135, Mar. 2006.

[4] J. Dai, D. Xu, and B. Wu, "A novel control scheme for current–source–converter-based PMSG wind energy conversion systems," IEEE Trans.Power Electron., vol. 24, no. 4, pp. 963–972, Apr. 2009.

[5] J. Birk and B. Andresen, "Parallel-connected converters for optimizingefficiency, reliability and grid harmonics in a wind turbine," in Proc.EPE'07 Conf., Aalborg, Denmark, Sep. 2007, pp. 1–7.

[6] Z. Xu, R. Li, H. Zhu, D. Xu, and C. H. Zhang, "Control of parallel multipleconverters for direct-drive permanent-magnet wind power generationsystems," IEEE Trans. Power Electron., vol. 27, no. 3, pp. 1250–1270,Mar. 2012.

[7] W. Erdman and M. Behnke, "Low wind speed turbine project phase II: Theapplication of medium-voltage electrical apparatus to the class of variablespeed multi-megawatt low wind speed turbines," San Ramon, CA, USA,Natl. Renew. Energy Lab. Rep., NREL/SR-500-38686, Nov. 2005.

[8] H. Abu-Rub, J. Holtz, J. Rodriguez, and G. Baoming, "Medium-voltagemultilevel converters-state of the art, challenges and requirements inindustrial applications," IEEE Trans. Ind. Electron., vol. 57, no. 8,pp. 2581–2596, Aug. 2010.

[9] R. C. Portillo, M. M. Prats, J. I. Leon, J. A. Sanchez, J. M. Carrasco,E. Galvan et al., "Modelling strategy for back-to-back three-level convertersapplied to high-power wind turbines," IEEE Trans. Ind. Electron.,vol. 53, no. 5, pp. 1483–1491, Oct. 2006.

[10] E. J. Bueno, S. Cóbreces, F. J. Rodríguez, A. Hernández, and F. Espinosa,"Design of a back-to-back NPC converter interface for wind turbines with Squirrel-cage induction generator," IEEE Trans. Energy Convers., vol. 23,no. 3, pp. 932–945, Sep. 2008.

[11] A. Faulstich, J. K. Steinke, and F. Wittwer, "Medium voltage converter forpermanent magnet wind power generators up to 7 MW," in Proc. EPEConf., Barcelona, Spain, Sep. 2009, pp. 9–17.

[12] C. L. Xia, X. Gu, and Y. Yan, "Neutral-point potential balancing of threelevelinverters in direct-driven wind energy conversion system," IEEETrans. Energy Convers., vol. 26, no. 1, pp. 18–29, Mar. 2011.

[13] M. Winkelnkemper, F. Wildner, and P. K. Steimer, "6 MVA five-levelhybrid converter for wind power," in Proc. IEEE PESC'08 Conf., Rhodes,Greece, Jun. 2008, pp. 4532–4538.

[14] X. Yuan, J. Chai, and Y. Li, "A transformer-less high-power converter forlarge permanent magnet wind generator systems," IEEE Trans. Sustain.Energy, vol. 3, no. 3, pp. 318–329, Jul. 2012.

[15] C. Xia, Z. Wang, T. Shi, and Z. Song, "A novel cascaded boost chopper forthe wind energy conversion system based on the permanent magnet synchronous generator," IEEE Trans. Energy Convers., vol. 28, no. 3,pp. 512–522, Sep. 2013.

[16] C.H. Ng,M. A. Parker, R. Li, P. J. Tavner, J. R. Bumby, and E. Spooner, “Amultilevelmodular converter for a large lightweightwind turbine generator,”IEEE Trans. Power Electron., vol. 23, no. 3, pp. 1062–1074, May 2008.

[17] M. A. Parker, C. H. Ng, and L. Ran, “Fault-tolerant control for a modulargenerator converter scheme for direct drive wind turbines,” IEEE Trans.Ind. Electron., vol. 58, no. 1, pp. 305–315, Jan. 2011.

[18] J. Kang, N. Takada, E. Yamamoto, and E. Watanabe, “High power matrixconverter for wind power generation applications,” in Proc. ICPE ECCE Asia Conf., Jeju, Korea, Jun. 2011, pp. 1331–1336.

[19] M. A. Perez, J. R. Espinoza, J. R. Rodriguez, and P. Lezana, “Regenerativemedium voltage AC drive based on a multicell arrangement with reducedenergy storage requirements,” IEEE Trans. Ind. Electron., vol. 52, no. 1,pp. 171–180, Feb. 2005.

[20] S. Inoue and H. Akagi, “A bidirectional isolated dc–dc converter as a corecircuit of the next-generation medium-voltage power conversion system,”IEEE Trans. Power Electron., vol. 22, no. 2, pp. 535–542, Mar. 2007.

[21] F. Iov, F. Blaabjerg, J. Clare, O. Wheeler, A. Rufer, and A. Hyde,“UNIFLEX-PM-A key-enabling technology for future European electricitynetworks,” EPE J., vol. 19, no. 4, pp. 6–16, 2009.

[22] J. Rodriguez, S. Bernet, B. Wu, J. O. Pontt, and S. Kouro, “Multilevelvoltage source converter topologies for industrial medium-voltage drives,”IEEE Trans. Ind. Electron., vol. 54, no. 6, pp. 2930–2945, Dec. 2007.

[23] H. D. Bang, R. P. Roojj, A. S. McDonald, and M. A. Mueller, “10MWwindturbine direct drive generator design with pitch or active speed stall control,”in Proc. IEEE IEMDC Conf., Antalya, Turkey, vol. 2, May 2007,pp. 1390–1395.

[24] X. Yuan, F. Wang, D. Boroyevich, Y. Li, and R. Burgos, “Dc-link voltagecontrol of a full power converter for wind generator operating in weak-gridsystems,” IEEE Trans. Power Electron., vol. 24, no. 9, pp. 2178–2192,Sep. 2009.

[25] R. Cardenas and R. Pena, “Sensor less vector control of induction machinesfor variable-speed wind energy applications,” IEEE Trans. Energy Convers.,vol. 19, no. 1, pp. 196–205, Mar. 2004.

[26] P. J. Tavner, G. J. W. Bussel, and F. Spinato, “Machine and converterreliabilities in wind turbines,” in Proc. IET PEMD’06 Conf., Dublin,Ireland, Mar. 2006, pp. 127–130.

[27] R. Teodorescu, F. Blaabjerg, M. Liserre, and P. C. Loh, “Proportionalresonantcontrollers and filters for grid-connected voltage–sourceconverters,” IEE Proc. Elect. Power Appl., vol. 153, no. 5, pp. 750–762,Sep. 2006.

[28] R. Teodorescu,M. Liserre, and P. Rodriguez, Grid Converters for Photovoltaicand Wind Power Systems, Chap. 4. Hoboken, NJ, USA: Wiley, 2011.

[29] IGBT module datasheet [Online]. Available: http://www.infineon.comdgdl/

[30] S. Dieckerhoff, S. Bernet, and D. KrugPower, “Loss-oriented evaluation ofhigh voltage IGBTs and multilevel converters in transformerless tractionapplications,” IEEE Trans. Power Electron., vol. 20, no. 6, pp. 1328–1336,
Nov. 2005.

ISSN No: 2348-4845
International Journal & Magazine of Engineering, Technology, Management and Research
*A Peer Reviewed Open Access International Journal*

Mr. V.Rajesh he is pursuing M.Tech (Power Electronics) at Dhruva Institute Of Engineering And Technology.Completed His B.Tech(EEE) From New Nethaji Institute Of Engineering And Technology Nalgonda, TELANGANA STATE,INDIA

**Mr.V.BALU** he received M.E (Power Systems) from University College of Engineering, Osmania University, Hyderabad in 2008 A.P. Graduated from JNTU University, Hyderabad in the year 2002. Presently he is working as Assistant Professor in Dhruva Institute of Engineering & Technology, Hyderabad in the Department of Electrical & Electronics Engineering. He had total 9 years of experience in teaching. His fields of interest include power quality and Power Systems Optimization.